

# Whole-brain activation signatures of weight-lowering drugs



Henrik H. Hansen<sup>\*1</sup>, Johanna Perens<sup>1</sup>, Urmas Roostalu, Jacob Lercke Skytte, Casper Gravesen Salinas, Pernille Barkholt, Ditte Dencker Thorbek, Kristoffer T.G. Rigbolt, Niels Vrang, Jacob Jelsing, Jacob Hecksher-Sørensen<sup>\*\*</sup>

## ABSTRACT

**Objective:** The development of effective anti-obesity therapeutics relies heavily on the ability to target specific brain homeostatic and hedonic mechanisms controlling body weight. To obtain further insight into neurocircuits recruited by anti-obesity drug treatment, the present study aimed to determine whole-brain activation signatures of six different weight-lowering drug classes.

**Methods:** Chow-fed C57BL/6J mice ( $n = 8$  per group) received acute treatment with lorcaserin (7 mg/kg; i.p.), rimonabant (10 mg/kg; i.p.), bromocriptine (10 mg/kg; i.p.), sibutramine (10 mg/kg; p.o.), semaglutide (0.04 mg/kg; s.c.) or setmelanotide (4 mg/kg; s.c.). Brains were sampled two hours post-dosing and whole-brain neuronal activation patterns were analysed at single-cell resolution using c-Fos immunohistochemistry and automated quantitative three-dimensional (3D) imaging.

**Results:** The whole-brain analysis comprised 308 atlas-defined mouse brain areas. To enable fast and efficient data mining, a web-based 3D imaging data viewer was developed. All weight-lowering drugs demonstrated brain-wide responses with notable similarities in c-Fos expression signatures. Overlapping c-Fos responses were detected in discrete homeostatic and non-homeostatic feeding centres located in the dorsal vagal complex and hypothalamus with concurrent activation of several limbic structures as well as the dopaminergic system.

**Conclusions:** Whole-brain c-Fos expression signatures of various weight-lowering drug classes point to a discrete set of brain regions and neurocircuits which could represent key neuroanatomical targets for future anti-obesity therapeutics.

© 2021 The Author(s). Published by Elsevier GmbH. This is an open access article under the CC BY-NC-ND license (<http://creativecommons.org/licenses/by-nc-nd/4.0/>).

**Keywords** Imaging; iDISCO; Light sheet fluorescence microscopy; c-Fos; Obesity; Anti-Obesity drugs

## 1. INTRODUCTION

Obesity represents a complex medical and behavioural problem which is insufficiently managed by current treatment interventions. Over the past decades, it has become increasingly clear that the brain plays a fundamental role in regulating energy balance and body weight homeostasis. Central control of eating and energy balance is determined by a rich interplay of humoral, neuronal and molecular mechanisms. Peripheral signals of metabolic status, such as circulating factors (macronutrients, endocrine hormones) and neural innervation (vagal sensory nerves), activate distinct brain areas in a highly organised, hierarchical fashion. The involved central nervous system (CNS) circuits are regulated by both central and peripheral neurotransmitters, including hormones, neuropeptides, catecholamines and other endogenous ligands acting on specific receptor systems that regulate homeostatic and hedonic pathways [1]. The hypothalamus is considered one of the most important target structures for blood-borne hormonal and metabolic factors [2]. Also, there is ample evidence to support a key role for circumventricular organs, specialised brain

structures with extensive vascularisation and fenestration, in sensing and relaying interoceptive signals of the nutritional state from the gut and viscera. Among these sensory areas, the brainstem dorsal vagal complex (DVC) is ideally positioned to transduce peripheral metabolic signals [3]. The executive control of food intake involves the cortico-limbic system receiving homeostatic signals relayed from the hypothalamus, amygdala and brainstem [4]. Many of the neurocircuits and hormones known to underlie the sensations of hunger and satiety also alter the activity in neural pathways controlling cue-potentiated feeding, pleasure and reward. In particular, the dopaminergic system has been implicated in the motivational and hedonic aspects of eating [5,6]. Excess caloric intake leading to obesity may therefore be conceptualised as the integral effects of deficient appetite regulation and eating-related impulse control [7]. Accordingly, neuroimaging studies in obese patients have linked efficient weight loss to altered activity in key brain sites for control of autonomic, executive and hedonic signalling [8].

The search for effective weight-lowering therapies has resulted in the development of obesity therapeutics with various modes and sites of

Gubra, Hørsholm, Denmark

<sup>1</sup> Henrik H. Hansen and Johanna Perens contributed equally to this work.

\*Corresponding author. Gubra, Hørsholm Kongevej 11B, DK-2970 Hørsholm, Denmark. Tel. +45 31 52 26 50. E-mail: [hbh@gubra.dk](mailto:hbh@gubra.dk) (H.H. Hansen).

\*\*Corresponding author. Gubra, Hørsholm Kongevej 11B, DK-2970 Hørsholm, Denmark. Tel. +45 29 86 94 07. E-mail: [jhs@gubra.dk](mailto:jhs@gubra.dk) (J. Hecksher-Sørensen).

Received November 20, 2020 • Revision received January 21, 2021 • Accepted January 21, 2021 • Available online 30 January 2021

<https://doi.org/10.1016/j.molmet.2021.101171>

**Abbreviations**

AAA	anterior amygdalar area	LP	lateral posterior nucleus of the thalamus
ACB	nucleus accumbens	LPO	the lateral preoptic nucleus
APN	anterior pretectal nucleus	LSFM	light sheet fluorescence microscopy
ARH	arcuate hypothalamic nucleus	MD	mediodorsal nucleus of the thalamus
AP	area postrema	MDRNd	dorsal medullary reticular nucleus
BLA	basolateral amygdalar nucleus	MPO	medial preoptic nucleus
BST	bed nuclei of the stria terminalis	MY-mot	motor related part of medulla
CA3	field CA3 of the Ammon's horn	NTS	nucleus of the solitary tract
CEA	central amygdalar nucleus	PARN	parvocellular reticular nucleus
CLA	claustrum	PB	parabrachial nucleus
DG	dentate gyrus	PH	posterior hypothalamic nucleus
DMH	dorsomedial nucleus of the hypothalamus	PO	peroral
DMX	dorsal motor nucleus of the vagus nerve	PPT	posterior pretectal nucleus
DVC	dorsal vagal complex	PS	parastriatal nucleus
iDISCO	immunolabelling-enabled imaging of solvent-cleared organs	PSTN	parasubthalamic nucleus
EP	endopiriform nucleus	pTFCE	probabilistic threshold-free cluster enhancement
FDR	false discovery rate	PVH	paraventricular hypothalamic nucleus
FWER	family-wise error rate	PVT	paraventricular nucleus of the thalamus
G3DE	Gubra 3D Experience data viewer	SC	subcutaneous
HIP	hippocampal region	SCm	motor related superior colliculus
IMD	intermediodorsal nucleus of the thalamus	SGN	thalamic suprageniculate nucleus
IP	intraperitoneal	SNC	substantia nigra pars compacta
IRN	intermediate reticular nucleus	SUM	supramammillary nucleus
IMD	intermediodorsal nucleus of the thalamus	TU	tuberomammillary nucleus
LA	lateral amygdalar nucleus	VMH	ventromedial hypothalamic nucleus
LGv	ventral part of the lateral geniculate complex	VPLpc	parvocellular part of the ventroposteromedial thalamic nucleus
LHA	lateral hypothalamic area	VTA	ventral tegmental area
		ZI	zona incerta

CNS action. Most, if not all, centrally acting anti-obesity therapeutics act as appetite suppressants or curb food reward sensitivity [9,10]. Existing medicines to combat the obesity epidemic are, however, disappointingly few in number as drug development for obesity has been notoriously difficult due to insufficient clinical efficacy or safety concerns [11]. The few compounds that promote significant weight loss are associated with adverse side effects that cause treatment discontinuation or prevent long-term therapy in obese patients [12]. Understanding of peptide receptor function in regulating energy balance has evolved considerably in the past few years, which has resulted in an increased focus on developing modified gut peptides and neuropeptides as anti-obesity drugs [13].

The increasing number of weight-lowering drugs characterised in obese patients provides unique insights into shared and specific CNS responses to the various drug classes. Given the highly different molecular mechanisms targeted by centrally acting anti-obesity therapeutics, a scrutinised comparative analysis would optimally require imaging of the CNS pharmacological effects on a brain-wide scale. Methods for imaging deep within transparent organs has proven instrumental for unbiased mouse whole-brain mapping and quantitation of brain activation patterns at single-cell resolution using c-Fos expression as a proxy for neuronal stimulation [14]. Here, we mapped and compared mouse whole-brain c-Fos expression signatures of six centrally acting weight-lowering drugs with documented clinical effect, including lorcaserin (Belviq, 5-HT<sub>2C</sub> receptor agonist), rimonabant (Acomplia, cannabinoid CB<sub>1</sub> receptor antagonist), bromocriptine (Parlodel, dopamine D<sub>2</sub> receptor agonist), sibutramine (Meridia, dual noradrenaline-serotonin reuptake inhibitor), semaglutide (Ozempic, glucagon-like peptide-1 (GLP-1) receptor agonist) and setmelanotide (RM-493, melanocortin-4 receptor (MC4R) agonist) [9,13,15]. Our

study pinpoints brain regions and nuclei which could represent critical targets for future anti-obesity therapeutics.

## 2. MATERIALS AND METHODS

### 2.1. Animals

The Danish Animal Experiments Inspectorate approved all experiments which were conducted according to internationally accepted principles for the use of laboratory animals (license #2013-15-2934-00784). Male C57Bl/6J mice (9 weeks old, n = 80) were from Janvier Labs (Le Genest Saint Isle, France) and housed in a controlled environment (12-h light/dark cycle, lights on at 3 AM, 21 ± 2 °C, humidity 50 ± 10%). Each animal was identified by an implantable subcutaneous microchip (PetID Microchip, E-vet, Haderslev, Denmark). Mice had ad libitum access to tap water and regular chow (Altromin 1324, Brogaarden, Hørsholm, Denmark) throughout the study and were acclimatised for one week before study start.

### 2.2. Drug treatment

The study was conducted in the light phase. Mice were single-housed and randomized to treatment based on body weight recorded one day before treatment start. Compounds included lorcaserin hydrochloride hemihydrate (Adooq Bioscience, Irvine, CA); rimonabant hydrochloride (Chemos GmbH, Regenstauf, Germany); bromocriptine mesylate (Toronto Research Chemicals, Toronto, ON, Canada); sibutramine (AH Diagnostics, Aarhus, Denmark); semaglutide (Hoersholm Pharmacy, Hoersholm, Denmark) and setmelanotide hydrochloride (MetChemExpress, Monmouth Junction, NJ). Vehicles were as follows: 0.1% Tween-80 in saline (vehicle IP1, for lorcaserin); 5% dimethylsulfoxide + 5% chremophor in saline

(vehicle IP2, for rimonabant and bromocriptine), 0.5% hydroxypropyl methylcellulose (vehicle PO, for sibutramine), phosphate-buffered saline + 0.1% bovine serum albumin (vehicle SC, for semaglutide and setmelanotide). Mice ( $n = 8$  per group) were dosed with lorcaserin (7 mg/kg, 36  $\mu\text{mol/kg}$ , i.p.), rimonabant (10 mg/kg, 22  $\mu\text{mol/kg}$ , i.p.), bromocriptine (10 mg/kg, 15  $\mu\text{mol/kg}$ , i.p.), sibutramine (10 mg/kg, 36 mmol/kg, p.o.), semaglutide (0.04 mg/kg, 9.7 nmol/kg, s.c.) or setmelanotide (4 mg/kg, 3.5  $\mu\text{mol/kg}$ , s.c.). Doses were corrected for individual salt weight. Corresponding control groups were administered vehicle (5 ml/kg, i.p., s.c. or p.o.). All compounds were prepared fresh and administered during the light phase.

### 2.3. Tissue processing

Mice were sedated with 2–4% isoflurane/O<sub>2</sub> (Attane Vet., ScanVet Animal Health, Fredensborg, Denmark) inhalation, anaesthetised by Hypnorm-Dormicum (fentanyl 788  $\mu\text{g/kg}$ , fluanisone 25 mg/kg and midazolam 12.5 mg/kg, s.c.) and transcardially perfused with heparinized PBS and 10% neutral-buffered formalin. Brain samples were collected, prepared, immunolabelled and cleared according to the iDISCO+ protocol [16,17] as described in [18] using identical reagents and antibodies.

### 2.4. Light sheet microscopy

Brains were imaged in axial orientation using a Lavisision ultramicroscope II (Miltényi Biotec GmbH, Bergisch Gladbach, Germany) with Zyla 4.2P-CL10 sCMOS camera (Andor Technology, Belfast, United Kingdom), SuperK EXTREME supercontinuum white-light laser EXR-15 (NKT photonics, Birkerød, Denmark) and MV PLAPO 2XC (Olympus, Tokyo, Japan) objective lens. Horizontal images were acquired at 0.63 $\times$  magnification (1.2  $\times$  total magnification) with an exposure time of 254 ms in a z-stack at 10  $\mu\text{m}$  intervals. Acquired volumes (16-bit tiff) had an in-plane resolution of 4.8  $\mu\text{m}$  and a z-resolution of 3.78  $\mu\text{m}$  (NA = 0.156). Data were acquired in two channels, autofluorescence at 560  $\pm$  20 nm (excitation) and 650  $\pm$  25 nm (emission) wavelength (80% laser power) and c-Fos staining at 630  $\pm$  15 nm (excitation) wavelength and 680  $\pm$  15 nm (emission).

### 2.5. Image analysis

Image processing, registration and cell detection was performed according to the method by Perens et al. [18]. Identification of c-Fos+ cells involved detection of local intensity peaks within a moving filter cube of 5  $\times$  5  $\times$  3 pixels and seeded watershed segmentation (background intensity cut-off of 400 for specific channel, size of watershed segmentation volumes between 8 and 194 voxels), whereas detected intensity peaks were used as seeds. For cell quantification per brain region, light sheet fluorescence microscopy (LSFM) atlas was aligned to the individual cell segmentation volumes via pre-processed autofluorescence volumes through affine and b-spline transformations. Heatmaps depicting the up- and downregulation of c-Fos expression were created by aligning the cell-segmentation volumes to the LSFM-based mouse brain atlas using the inverse transform, generating and summing Gaussian spheres ( $\sigma = 2$  voxels) around the centres of the c-Fos positive cells followed by subtraction of the average vehicle heatmaps from the group average heatmaps and removing the signal from non-significant brain regions based on the results of region-based statistical analysis. Image processing was performed in Python, and the Elastix software was applied to implement the registrations [19,20]. All registrations utilised mutual information as a

similarity measure. 3D visualizations of heatmaps were created with the microscopy image analysis software Imaris™ version 2 (Oxford instruments, Abingdon, UK).

### 2.6. Region-based statistics

Statistical analysis of the c-Fos cell counts was performed in 308 atlas-defined brain regions, which were created by merging the 666 region segmentations of the LSFM mouse brain atlas according to a hierarchy tree of the atlas ontology [18,21]. A generalised linear model (GLM) was fitted to the number of detected c-Fos positive cells in each brain region in every animal group using a negative binomial for modelling the distribution of the datapoints. For each GLM, a Dunnett's test was performed. Due to the large number of regions in which the statistical test was performed, Benjamin-Hochberg false discovery rate (FDR) correction (cut-off of 0.05) was packaged on the p-values. Statistical analysis was performed using R packages MASS, multcomp, lmerTest and car [22–26]. Subsequently, a two-step manual validation was conducted to verify that the datapoints follow the negative binomial distribution, significance of the regions is not achieved due to outliers and the signal is not resulting from a spillover from neighbouring regions. The former was done by investigating deviance residuals and discarding significant regions if the residuals are violating the assumptions of normality and homoscedasticity. To quantify the influence of individual data points, Cook's distance was calculated, and significant regions with overly influential data points were discarded. Finally, origins of the signals were visually studied in the remaining significant regions and if spillover was identified, the region was declared as not significant. Two animals (vehicle SC, setmelanotide treatment) were excluded from the region-based statistical analysis due to suboptimal tissue quality.

### 2.7. Voxel-based statistics

Voxel-based statistical analysis was performed on the cell segmentation volumes. The pre-processing followed the approach by Vandenberghe et al. [27] for converting binary segmentation volumes of immunostained markers into Gaussian random fields which enable signal comparisons on a voxel level. First, the segmentation volumes were converted to the LSFM-based mouse brain atlas space. Subsequently, signal occurring in low-density areas (1 cell per 100  $\mu\text{m}^3$  in average per group comparison for the hindbrain and cerebellum, and 1–5 cells per 100  $\mu\text{m}^3$  for the cerebrum, midbrain and interbrain) was excluded from the analysis. Gaussian background noise ( $\mu = 0$ ,  $\sigma = 0.1$ ) was added to the binary cell segmentation volumes, and the volumes underwent smoothing with a Gaussian kernel with an optimal standard deviation ( $\sigma = 2.25$ ) determined via bootstrap error minimization [27]. The last step of the pre-processing involved averaging the smoothed cell segmentations of the right and left hemisphere to improve statistical power. Voxel-wise statistical analysis was performed according to the probabilistic threshold-free cluster enhancement (pTFCE) method [28], while the hindbrain and cerebellum were analysed separately from the cerebrum, interbrain and midbrain. Standard values were used for the parameters  $N_h$  (number of thresholds),  $Z_{\text{est}}$  (cluster-forming threshold) and  $C$  (connectivity) when performing pTFCE analysis. Family-wise error rate (FWER) was applied for multiple comparisons adjustments. Four animals were excluded from the voxel-based statistical analysis: the same two animals which were removed from the region-based statistical analysis and two additional mice from the bromocriptine-dosed group due to extremely low total cell counts.

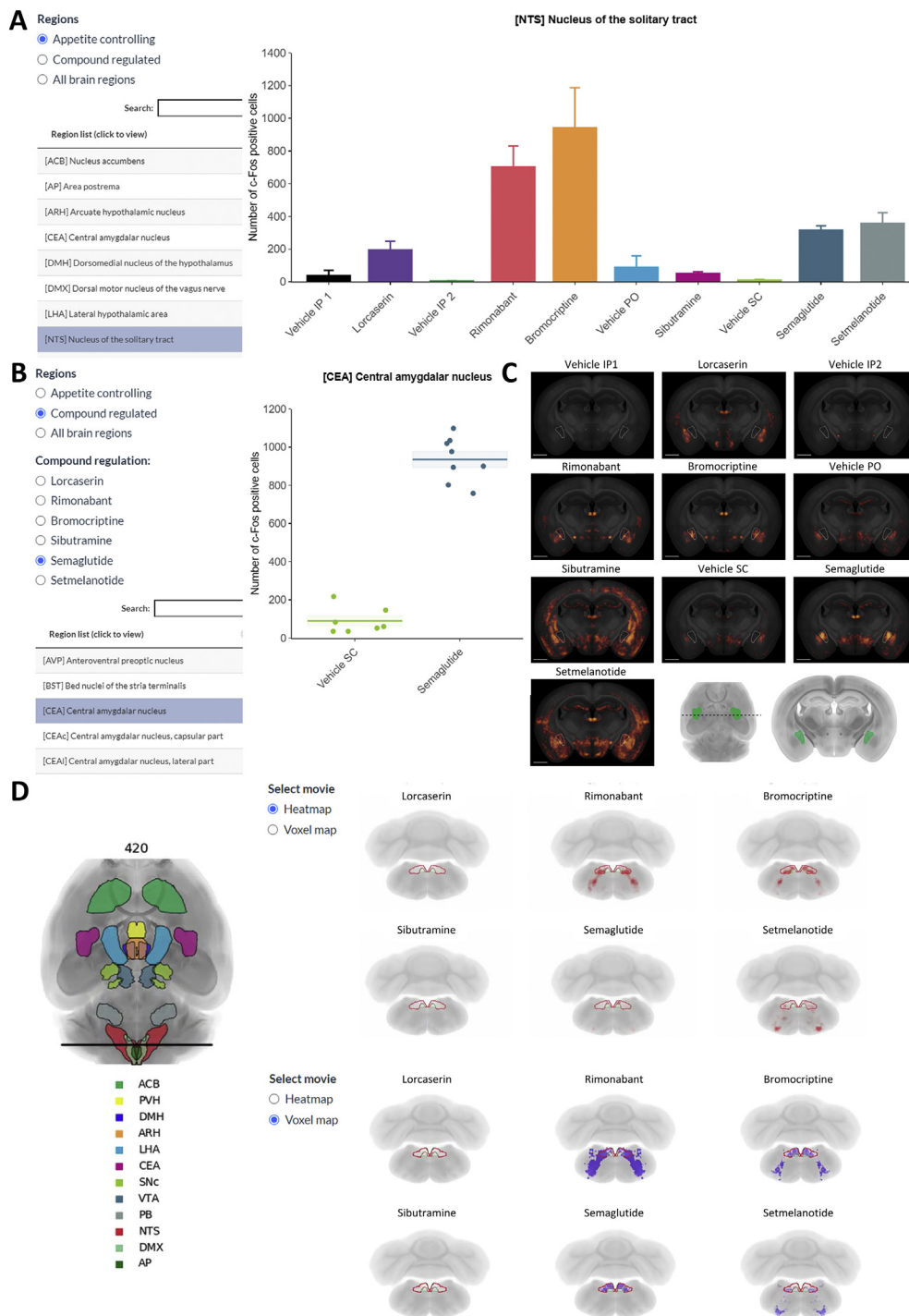


**Figure 1: Web-based whole-brain imaging data viewer** (Gubra 3D Experience/G3DE, <https://g3de.gubra.dk/>). **(A)** User interface of the online data browsing system showing the quantitative data for all treatment groups in selected appetite-regulating brain region (nucleus of the solitary tract, NTS). **(B)** Brain regions with compound-induced statistically significantly regulation of c-Fos+ cell numbers ( $p < 0.05$  vs. corresponding vehicle control group). Example of data filtered to show only semaglutide-induced regulation of c-Fos expression (c-Fos+ cell counts) in the central amygdalar nucleus (CEA) in each individual mouse (dot plot with indication of average number of c-Fos+ cells  $\pm$  S.E.M.). **(C)** Representative group-average c-Fos expression heatmaps for each individual drug tested. *Lower panel:* Corresponding dorsal and coronal view of selected brain region. **(D)** Online movies showing whole-brain c-Fos responses to weight-lowering drugs (selected coronal plane at the level of the nucleus of the solitary tract, NTS). The 12 appetite-regulating regions are delineated in the coronal slice-by-slice fly-through movies. *Upper panel:* Heatmaps showing vehicle-subtracted average whole-brain c-Fos expression in response to weight-lowering compounds. Statistically significant changes ( $p < 0.05$ ; Dunnett's test negative binomial generalized linear model, FDR  $< 0.05$  for p-value adjustment) in c-Fos expression in response to treatment with weight-lowering compounds compared to corresponding vehicle controls are depicted in red (upregulation) and blue (downregulation). *Lower panel:* P-value maps from voxel-based statistical analysis visualising whole-brain c-Fos responses to individual weight-lowering drugs. Statistically significant changes between the treatment and vehicle group ( $p < 0.05$ ) are indicated by graded purple colour.

### 3. RESULTS

#### 3.1. Web-based imaging data viewer

All data are accessible using a web-based 3D imaging data viewer (Gubra 3D Experience/G3DE, <https://g3de.gubra.dk/>) allowing fast and efficient data mining as well as 3D visualisation of individual whole-brain c-Fos expression signatures of the drugs tested. The viewer provides users the opportunity to look up individual regions and display the quantitative data for all the treatment groups (Figure 1A) and filter for regions with statistically significant response to drug treatment (Figure 1B). For selected regions, the anatomical location and representative heatmaps of group-average c-Fos expression are displayed for each treatment in common reference space (coronal view, Figure 1C). The viewer also includes fly-through movies with indication of significant up- and downregulation of c-Fos expression in response to compound administration according to region-based statistical analysis and p-value maps, respectively (Figure 1D).

#### 3.2. Brain-wide c-Fos expression profiles of weight-lowering drugs

Six weight-lowering drugs were profiled for acute effects on c-Fos expression patterns evaluated two hours after peripheral administration. Stimulated c-Fos expression, signifying neuronal activation, was a characteristic profile of all drugs tested. The drugs exhibited distinct whole-brain c-Fos expression signatures (Figure 2A–F). Accordingly, global c-Fos expression signatures of each individual drug were clearly separated (Figure 2G). The top 15 most influential brain regions driving the clustering of individual drug responses are indicated in Figure 2H. Out of 308 atlas-defined mouse brain areas analysed, the number of activated areas was most extensive for rimonabant (136 areas), setmelanotide (133 areas), lorcaserin (123 areas) and bromocriptine (96 areas). In comparison, brain activation patterns were more anatomically restricted for sibutramine (55 areas) and semaglutide (21 areas). Drug-induced c-Fos expression profiles also differed at the subregional level (see the G3DE data viewer).

#### 3.3. Activation of key brain areas involved in energy homeostasis and hedonic eating

The weight-lowering drugs showed differential effects in key brain areas regulating energy homeostasis and hedonic eating (Figure 3, G3DE data viewer). These 12 areas included cardinal hypothalamic feeding centres [paraventricular (PVH), dorsomedial (DMH) and arcuate (ARH) hypothalamic nucleus; lateral hypothalamic area, (LHA)]; central amygdalar nucleus (CEA); major dopaminergic pathways [nucleus accumbens (ACB), substantia nigra pars compacta (SNc), ventral tegmental area (VTA)] as well as components of the brainstem [parabrachial nucleus (PB), nucleus of the solitary tract (NTS), dorsal motor nucleus of the vagus nerve (DMX), area postrema (AP)]. A further detailed analysis included all significantly regulated brain areas (Figure 4, G3DE data viewer). The most notable c-Fos signals are summarised below, with special emphasis on overlapping features of the six weight-lowering drugs.

##### 3.3.1. Hypothalamus

Only setmelanotide induced c-Fos expression in all four designated subdivisions of the hypothalamus (PVH, DMH, ARH, LHA), see Figure 3. Lorcaserin, rimonabant, bromocriptine and setmelanotide significantly increased c-Fos + cell counts in the ARH and DMH, albeit to a different degree. Lorcaserin and setmelanotide also increased c-Fos + cell counts in the PVH. Rimonabant stimulated c-Fos expression in the LHA. Sibutramine and semaglutide showed no effect on c-Fos expression in

the PVH, DMH, ARH and LHA. With the exception of sibutramine, all drugs activated the paraventricular nucleus (PVH), paraventricular nucleus (PVT), intermediodorsal (IMD) and mediodorsal (MD) nuclei of the thalamus (Figure 4). Only rimonabant and setmelanotide showed additional effects in the ‘gustatory thalamus’ (parvocellular part of the ventroposteromedial thalamic nucleus (VPLpc, G3DE data viewer)). Lorcaserin, rimonabant, bromocriptine, sibutramine and setmelanotide stimulated c-Fos expression in visceral, limbic and primary gustatory cortical layers (Figures 2 and 4). Semaglutide did not influence c-Fos expression in any cortical areas examined.

##### 3.3.2. Thalamus and cerebral cortex

Several areas of the thalamus and cerebral cortex were influenced by treatments. Notably, all drugs increased c-Fos expression in the paraventricular (PVT), intermediodorsal (IMD) and mediodorsal (MD) nuclei of the thalamus (Figure 4). Only rimonabant and setmelanotide showed additional effects in the ‘gustatory thalamus’ (parvocellular part of the ventroposteromedial thalamic nucleus (VPLpc, G3DE data viewer)). Lorcaserin, rimonabant, bromocriptine, sibutramine and setmelanotide stimulated c-Fos expression in visceral, limbic and primary gustatory cortical layers (Figures 2 and 4). Semaglutide did not influence c-Fos expression in any cortical areas examined.

##### 3.3.3. Amygdala

All drugs robustly stimulated c-Fos expression in the amygdala, however, with drug-dependent subanatomical differences. Lorcaserin, rimonabant, bromocriptine, semaglutide and setmelanotide showed effects in the CEA. Whereas lorcaserin, rimonabant, bromocriptine and setmelanotide affected all parts of the CEA (central, medial, lateral), semaglutide only stimulated the medial part of the CEA (G3DE data viewer). With the exception of semaglutide, all drugs increased c-Fos expression in other amygdalar areas, such as the basolateral amygdalar nucleus (BLA), lateral amygdalar nucleus (LA) and anterior amygdalar area (AAA) (Figure 4). In the BLA, the effect of lorcaserin and sibutramine was located in the posterior/anterior part, while rimonabant, bromocriptine and setmelanotide affected all subdivisions (anterior, posterior, ventral; G3DE data viewer).

##### 3.3.4. Striatum and midbrain

With the exception of semaglutide, all drugs stimulated c-Fos expression in the ACB (Figure 3). Differences in drug responses were observed within distinct anatomical divisions of the ACB, *i.e.*, the shell and core (G3DE data viewer). The c-Fos signal was restricted to the shell (for lorcaserin, rimonabant, bromocriptine) or included both the shell and core (for sibutramine and setmelanotide). For other striatal areas affected, see Figure 4. With the exception of semaglutide, all other drugs stimulated c-Fos expression in the midbrain (Figure 4). While lorcaserin, rimonabant, bromocriptine and setmelanotide promoted c-Fos induction in the VTA, the SNc was refractory to all drugs tested (Figure 3). A subset of midbrain sensorimotor areas, including reticular nuclei, were also stimulated by lorcaserin, rimonabant, bromocriptine and setmelanotide.

##### 3.3.5. Brainstem

Semaglutide increased c-Fos expression in all four designated brainstem areas (AP, NTS, DMX, PB), see Figure 3. Notably, only semaglutide stimulated the AP. Semaglutide also induced c-Fos expression in Barrington’s nucleus, but showed no further effects in the brainstem (Figure 4). Both bromocriptine and setmelanotide increased c-Fos expression in PB, NTS and DMX. While rimonabant induced c-Fos in the PB and NTS, only the NTS responded to lorcaserin administration. Sibutramine did not influence c-Fos expression in the PB, NTS, DMX and AP (Figure 3). Other brainstem areas were activated by lorcaserin,

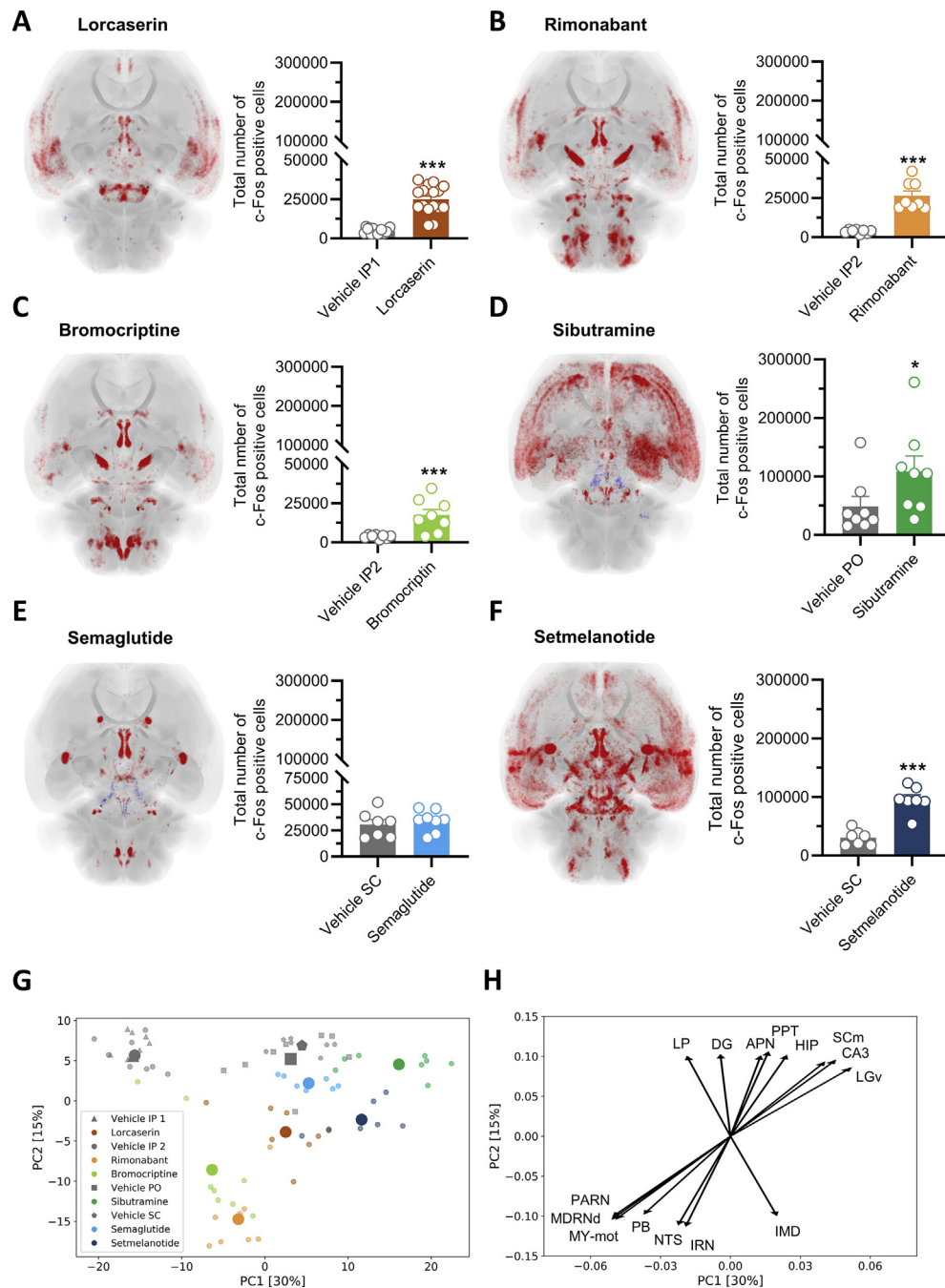


**Figure 2: 3D mapping and quantification of whole-brain c-Fos responses to acute treatment with various weight-loss promoting compounds.** Quantification and statistical analysis of c-Fos expression was performed in 308 brain regions. **(A)** Lorcaserin (7 mg/kg, i.p.), **(B)** rimonabant (10 mg/kg, i.p.), **(C)** bromocriptine (10 mg/kg, i.p.), **(D)** sibutramine (10 mg/kg, p.o.), **(E)** semaglutide (0.04 mg/kg, s.c.) and **(F)** setmelanotide (4 mg/kg, s.c.). All samples were registered into an LSFM-based mouse brain atlas. Heatmaps (dorsal view) depict vehicle-subtracted average whole-brain c-Fos expression ( $n = 7-8$  mice per group) responses to the individual drug. Brain areas with statistically significant changes in c-Fos expression ( $p < 0.05$ ; Dunnett's test negative binomial generalised linear model,  $FDR < 0.05$  for p-value adjustment) are delineated in red (upregulation) or blue (downregulation) compared to corresponding vehicle controls. Coronal slice-by-slice fly-through of the heatmaps can be found in the G3DE imaging viewer. Bar plots show the differences in total numbers of c-Fos+ cells detected in compound and corresponding vehicle-dosed mice (\* $p < 0.05$ , \*\*\* $p < 0.001$ ; Dunnett's test negative binomial generalised linear model). **(G)** Principal component analysis (PCA) of whole-brain c-Fos expression. The PCA plot illustrates the degree of separation between individual drug effects on global c-Fos expression patterns (large markers indicate group average). **(H)** PCA loading plot depicting the coefficients of the top 15 most influential brain regions driving the clustering of data points in PCA plot. **Abbreviations:** Vehicle IP1, 0.1% Tween-80 in saline (intraperitoneal); Vehicle IP2, 5% DMSO + 5% chremophor in saline (intraperitoneal); Vehicle PO, 0.5% hydroxypropyl methylcellulose (peroral); Vehicle SC, 0.1% bovine serum albumin in phosphate-buffered saline (PBS, subcutaneous); *PARN*, parvicellular reticular nucleus; *MDRNd*, dorsal medullary reticular nucleus; *MY-mot*, motor-related part of medulla; *PB*, parabrachial nucleus; *NTS*, nucleus of the solitary tract; *IRN*, intermediate reticular nucleus; *IMD*, intermediodorsal nucleus of the thalamus, *LP*, lateral posterior nucleus of the thalamus; *DG*, dentate gyrus; *LGv*, ventral part of the lateral geniculate complex; *APN*, anterior pretectal nucleus; *PPT*, posterior pretectal nucleus; *HIP*, hippocampal region; *SCm*, motor-related superior colliculus; *CA3*, field CA3 of the Ammon's horn.

rimonabant, bromocriptine, sibutramine and setmelanotide (Figure 4). For these drugs, most frequent overlapping effects were associated with activation of pontine and medullary reticular nuclei. Although the majority of drugs activated AP, NTS, DMX and PB, c-Fos responses were heterogeneous within these nuclei (Figure 1D, G3DE data viewer). To consider discrete changes in c-Fos + cell patterns not tracked by the atlas-guided analysis, we mapped changes in c-Fos+ cell clusters using label-free voxel-based statistical analysis. The p-value maps revealed different subanatomical responses to weight-lowering drugs (G3DE data viewer). For example, rimonabant, bromocriptine, semaglutide and setmelanotide activated large clusters of neurons in different segments of the PB (Figure 5). In contrast, c-Fos+ cell density did not change following administration of lorcaserin and sibutramine, signifying highly scattered c-Fos responses to these drugs.

### 3.3.6. Other areas

Overlapping drug effects were observed in subdivisions of the pallidum [bed nuclei of the stria terminalis (BST), substantia innominata] and subcortical plate [claustrum (CLA), endopiriform nucleus (EP)] (Figure 4). Drug effects were also detected within components of the hippocampal formation (Figure 4, G3DE data viewer).

## 4. DISCUSSION

Using c-Fos immunoreactivity as an indirect marker for neuronal activity, we mapped mouse whole-brain activation signatures of six individual weight-lowering drugs with different central mechanisms of action. A highly shared feature was activation of several nuclei and neurocircuits involved in the regulation of homeostatic feeding and food reward sensitivity. To facilitate the accessibility of the data presented here, a dedicated online interactive data browsing system was established. This resource will provide the community a platform for exploring the data in further detail and hopefully serve as the basis for future studies.

The largest overlap in c-Fos expression patterns was observed in the brainstem, amygdala, hypothalamus, thalamus and cortex. It is noteworthy that five out of six weight-lowering drugs stimulated components of the DVC, albeit showing anatomically distinct effects in the individual components (AP, NTS, DMX). Notably, weight-lowering drugs activating the DVC also activated the CEA and BST. Satiety signals arriving at the level of the dorsal vagal complex are distributed widely in the hypothalamus, amygdala and cortex [29]. Activation of the DVC triggers powerful satiety signals, which are conveyed by downstream feeding control circuitries, involving the PB, CEA and BST, to promote meal termination [30–32]. Large clusters of neurons in the medial/lateral NTS and lateral PB were activated by rimonabant, bromocriptine, semaglutide and setmelanotide. The NTS is a highly heterogeneous structure with several molecularly undefined neuron populations being recruited by anorexigenic drugs; however, NTS neurons communicate viscerosensory information to the PB as one important neural pathway in feeding control. Accordingly, recent experimental evidence indicates that activation of mid-caudal NTS neurons projecting to the lateral PB is sufficient to elicit satiety responses [30]. Because lorcaserin promoted highly dispersed c-Fos expression in the NTS without concurrent activation of the PB, it may be speculated that this induction pattern did not lead to coordinated NTS responses.

The hypothalamus is characterised by numerous connections with essentially every major part of the brain, including the brainstem, amygdala, thalamus, and hippocampus [33]. Hypothalamic mechanisms have been implicated in the weight-lowering properties of the

weight-lowering drug classes characterized in the present study [9,11]. Accordingly, five out of six weight-lowering drugs stimulated c-Fos expression in the hypothalamus, ranging from activation of few discrete nuclei (for semaglutide) to numerous nuclei across the entire hypothalamus (for setmelanotide). The PSTN, PS and SUM were activated by all drugs tested. The PSTN is rapidly activated by ingestion of palatable foods and has been proposed to suppress hedonic feeding behaviour via connections to the CEA and the insular cortex (AI) [34]. Also, the PS is an integral part of a satiety network involving the PB, CEA and AI [32]. The SUM has recently been identified as a neural substrate involved in relaying ghrelin-associated hunger signalling [35]. Cardinal hypothalamic areas engaged in feeding control and energy expenditure (ARH, DMH, LPO, MPO) were activated by most of the drugs tested. These areas are intimately connected and receive multiple humoral and neuronal inputs involved in energy homeostasis [33,36]. Less overlapping c-Fos profiles were observed for other prominent nutrient-sensing and feeding regulatory areas, such as the VMH, PVH and LHA [33]. Considering the melanocortin system plays an essential role in energy homeostasis [37], it is noteworthy that several of the weight-lowering drugs directly or indirectly stimulate melanocortin signalling pathways in specific areas of the hypothalamus (ARH) and brainstem (NTS) [38–40].

The weight-lowering drugs also activated medial/midline nuclei of thalamus (MD, PVT), which are principally connected to reciprocally activated corticolimbic (e.g., ORB, ILA) and limbic subcortical structures (e.g., BLA, ACB, BST). While the MD is closely involved in cognitive processes, PVT activation may encode palatable food reward associated with dopamine release in the ACB [41]. A subset of drugs showed combined stimulatory effects in the VPLpc ('gustatory thalamus') and GU, which forms a thalamocortical neurocircuit involved in taste processing [42].

CNS pathways regulating energy homeostasis are closely coupled with neurocircuits regulating food motivation and reward. Because the dopaminergic system is critically involved in hedonic feeding [5,6], we assessed whether drug-induced c-Fos signals also included dopaminergic areas in the striatum and midbrain. Four out of six drugs stimulated c-Fos expression in both the VTA and ACB. The VTA-ACB dopamine pathway is considered a key substrate for the incentive, reinforcing and motivational aspects of food intake [7]. The LHA-VTA-ACB loop has also been implicated in feeding and reward signalling [43]; however, LHA stimulation was not a common characteristic of the weight-lowering drugs tested. Almost all drugs stimulated the CLA, which receives dopamine inputs and transduces reward-associated signals to the ORB [44].

Brainstem and hypothalamic nuclei have classically been implicated in the appetite regulatory effects of GLP-1 receptor agonists [45], CB<sub>1</sub> receptor antagonists [46] and MC4R agonists [47]. The highly discrete c-Fos response to semaglutide is consistent with the peptide only accessing circumventricular/paraventricular areas [40]. Lack of blood–brain barrier penetrability of semaglutide suggests that c-Fos signals in deeper feeding centres, such as the ACB, BST, CEA and VTA, are secondary to direct effects in the hindbrain and hypothalamus. In the ARH, GLP-1 receptor agonist induced inhibition of food intake is mediated by direct activation of proopiomelanocortin/cocaine- and amphetamine-regulated transcript (POMC/CART) neurons and indirect inhibition of neuropeptide Y/agouti-related peptide (NPY/AgRP) neurons [48,49]. Despite ARH targeting of semaglutide, we and others have been unable to demonstrate enhanced arcuate c-Fos expression following treatment with semaglutide and liraglutide, a closely related analogue [40,50]. From these studies, it is unclear whether the lack of c-Fos response reflects opposing effects on POMC and NPY neuronal

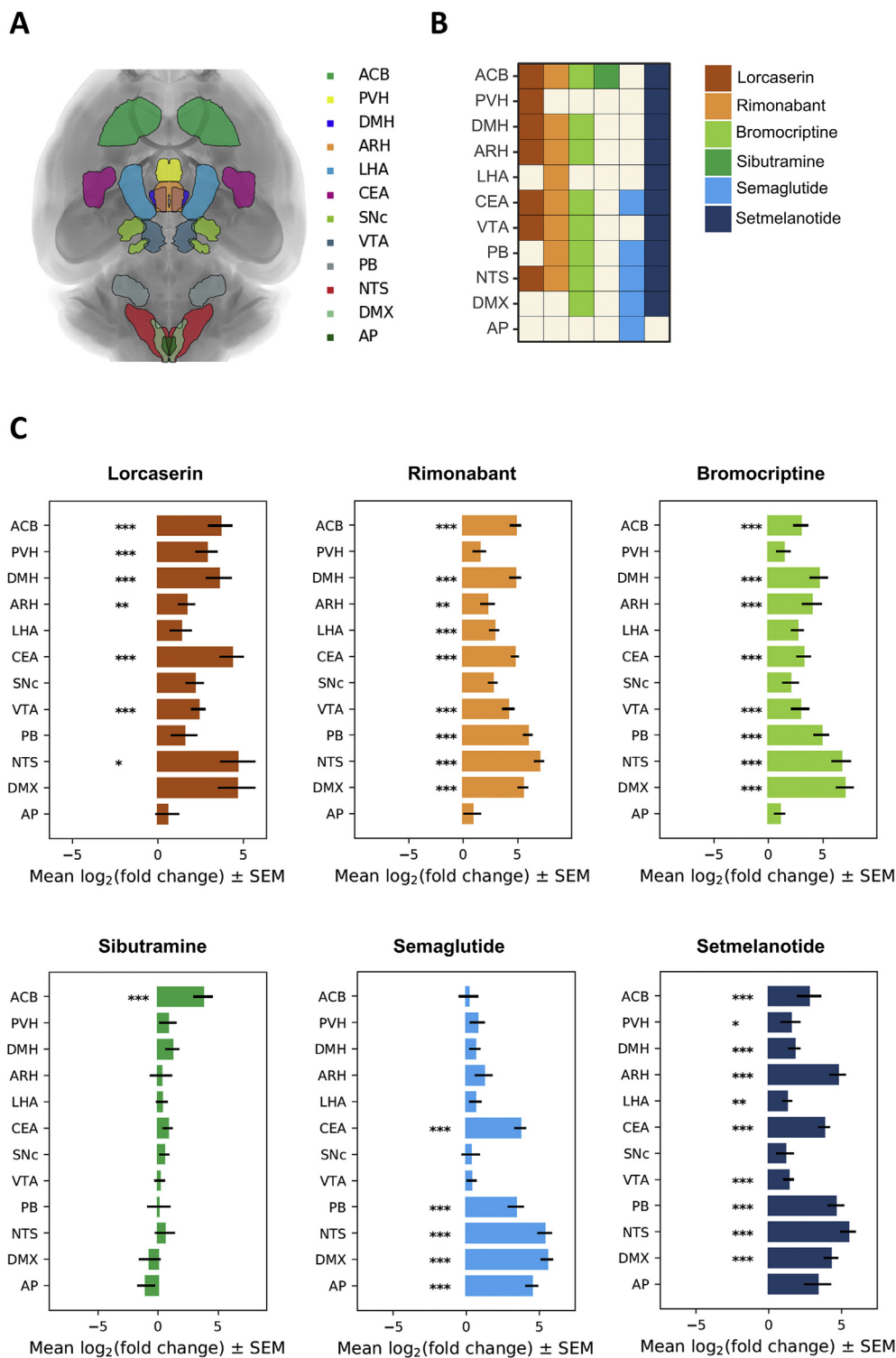


**Figure 3: Overlapping and specific c-Fos expression signatures of weight-lowering drugs in major appetite-regulating brain regions.** (A) Anatomical map (dorsal view) depicting 12 selected brain regions involved in appetite regulation. (B) Summary of drug-induced c-Fos induction across the 12 individual brain regions ( $p < 0.05$ ; Dunnett's test negative binomial generalised linear model, FDR  $< 0.05$  for p-value adjustment). (C) Fold-change ( $\log_2$  scale, mean  $\pm$  S.E.M.) in c-Fos positive cell counts in the 12 selected brain regions (rostral-caudal order) compared to corresponding vehicle controls. Dunnett's test negative binomial generalised linear model with p-value adjustment for multiple comparisons using FDR  $< 0.05$  was applied for statistical analysis (\* $p < 0.05$ ; \*\* $p < 0.01$ , \*\*\* $p < 0.001$ ). Abbreviations: *ACB*, nucleus accumbens; *ARH*, arcuate hypothalamic nucleus; *AP*, area postrema; *CEA*, central amygdalar nucleus; *DMH*, dorsomedial nucleus of the hypothalamus; *DMX*, dorsal motor nucleus of the vagus nerve; *LHA*, lateral hypothalamic area; *NTS*, nucleus of the solitary tract; *PB*, parabrachial nucleus; *PVH*, paraventricular hypothalamic nucleus; *SNC*, substantia nigra pars compacta; *VTA*, ventral tegmental area.

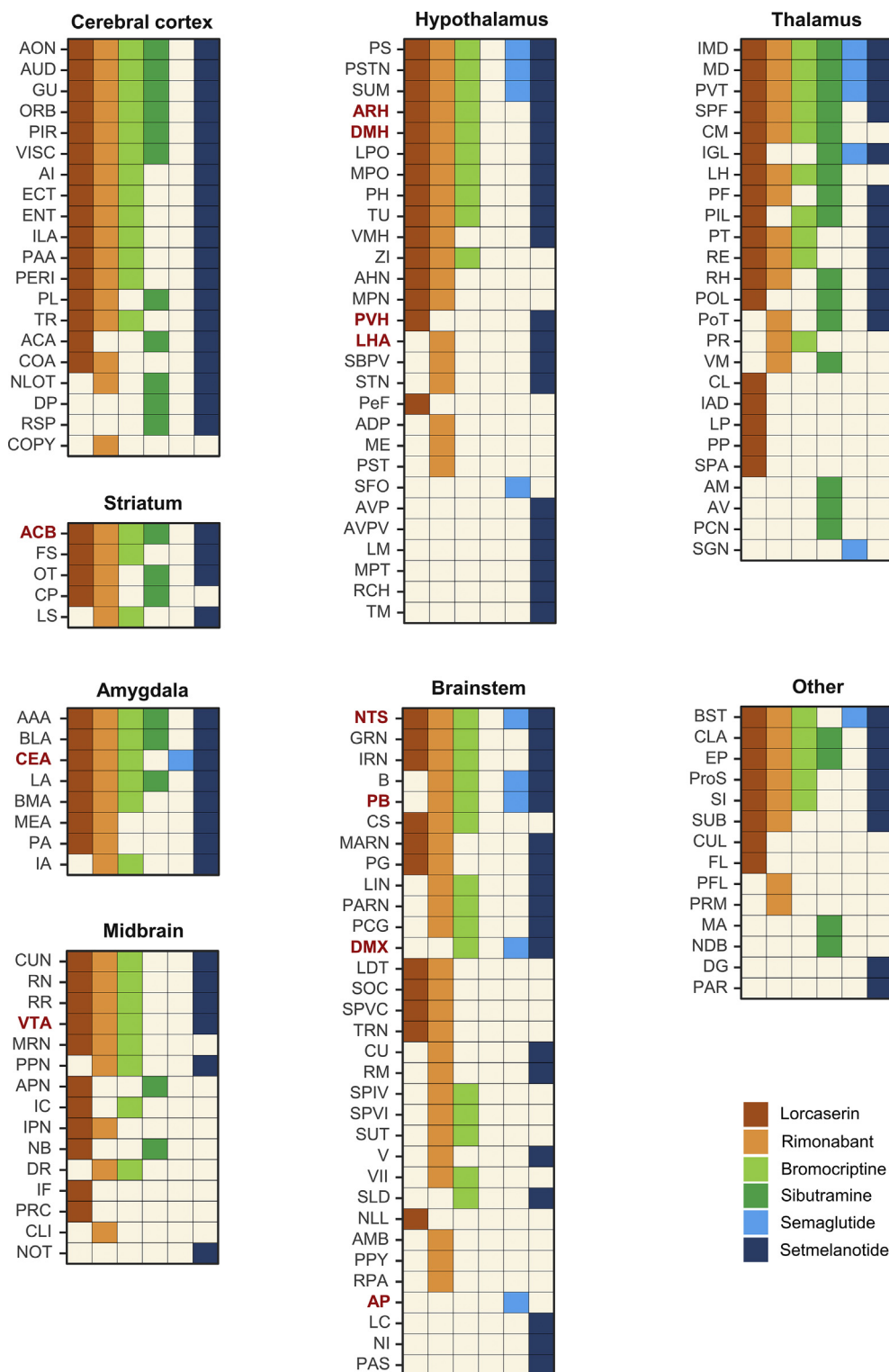


**Figure 4: Whole-brain c-Fos expression signatures in response to weight-lowering compounds.** Significant changes in c-Fos<sup>+</sup> cell counts ( $p < 0.05$ ) following administration of each individual weight-lowering compound. Dunnett's test negative binomial generalised linear model with p-value adjustment for multiple comparisons using FDR (cut-off of 0.05) was applied for statistical analysis. Regulated brain regions are categorised anatomically and ranked according to the number of drugs demonstrating a similar effect. With the exception of reduced c-Fos<sup>+</sup> cell counts in the thalamic suprageniculate nucleus (SGN, significantly down-regulated by liraglutide only), all significantly regulated areas exhibited increased c-Fos<sup>+</sup> cell counts following drug treatment as compared to corresponding vehicle controls. Major appetite-regulating regions are indicated in red (ACB, nucleus accumbens; ARH, arcuate hypothalamic nucleus; AP, area postrema; CEA, central amygdalar nucleus; DMH, dorsomedial nucleus of the hypothalamus; DMX, dorsal motor nucleus of the vagus nerve; LHA, lateral hypothalamic area; NTS, nucleus of the solitary tract; PB, parabrachial nucleus; PVH, paraventricular hypothalamic nucleus; VTA, ventral tegmental area). For other abbreviated brain regions, see the web-based imaging data viewer.

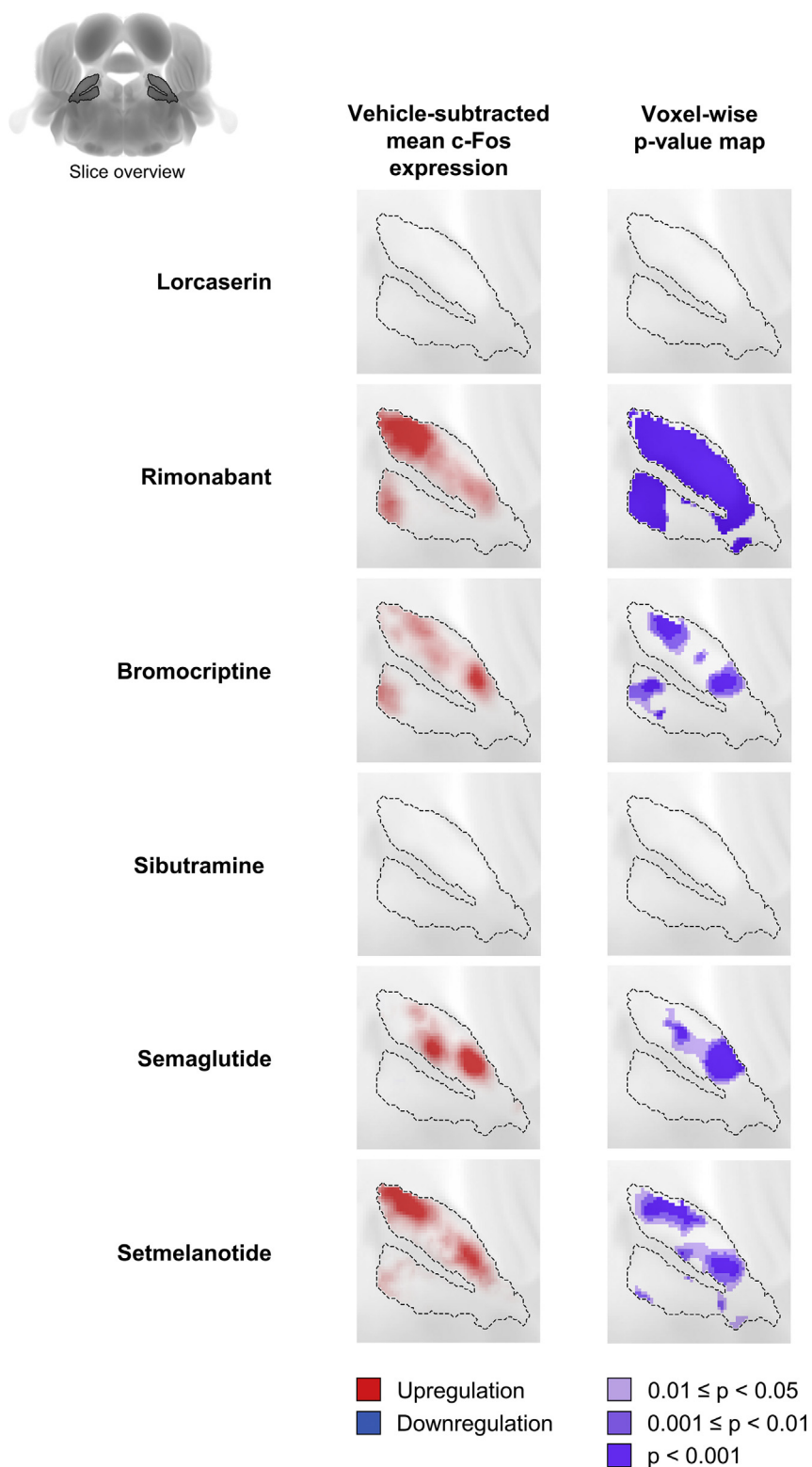


**Figure 5: Subregional differentiation of c-Fos responses in the parabrachial nucleus in response to weight-lowering compounds.** Voxel-wise statistical analysis of c-Fos expression was performed on pre-processed segmentation images of c-Fos+ cells using the pTFCE method and FWER approach for p-value adjustments. Resulting spatial p-value distributions ( $p < 0.05$ ) are shown for the parabrachial nucleus in a representative coronal cross-section for different compound treatments (right column). Levels of statistical significance are indicated by graded purple colours. Vehicle-subtracted group means of c-Fos expression are depicted in the left column (red, upregulation; blue downregulation as compared to corresponding vehicle controls). The signal appearing in the neighbouring regions of parabrachial nucleus has been marked on both p-value distribution and c-Fos expression visualizations for clarity. Coronal slice-by-slice fly-through of whole brain p-value distribution resulting from voxel-based statistical analysis is exemplified in [Figure 1D](#) and can be seen in the web-based imaging data viewer.

activity or whether peripherally administered GLP-1 receptor agonists may predominantly have indirect effects on ARH neurotransmission. Studies have also suggested role for GLP-1 receptors in the regulation of reward-associated circuits involving the ACB, VTA, LS and PVT [51]. Only the PVT, which projects to ACB and receives excitatory input from NTS [52], was activated by semaglutide.

In contrast to semaglutide, lorcaserin, bromocriptine, rimonabant and setmelanotide promoted extensive and brain-wide c-Fos responses, which could imply that these drugs have improved CNS accessibility and/or evoke amplified excitatory responses in targeted neurocircuits. Lorcaserin, rimonabant and setmelanotide promoted broad stimulatory effects in the hypothalamus, including the ARH, which is strongly linked to the appetite regulatory action of these compounds [38,39,46]. Also NTS neurons are important targets for achieving the full anorectic effect of 5-HT<sub>2C</sub> receptor stimulation [38]. In keeping with ARH-PVH connectivity being critical for the anorectic effects of MC4R agonists [39], setmelanotide also activated the PVH. The exact molecular mechanisms linking D<sub>2</sub> receptor activation to body weight regulation are unclear, but bromocriptine has been reported to promote satiation and thermogenesis via modulation of mesolimbic (ACB, VTA) and hypothalamic (LHA, ZI) dopaminergic signalling [53,54]. Lorcaserin, rimonabant and setmelanotide also stimulated c-Fos expression in ACB and VTA. Accumulating experimental evidence suggests that these compounds can reduce palatable food reward by indirect or direct action on ACB-VTA dopaminergic neurotransmission [55–57]. Although sibutramine did not evoke significant c-Fos stimulatory responses in the hypothalamus, available preclinical data suggest that sibutramine confers appetite suppression by enhancing adrenoceptor activity in ARC and LH [58]. In our study, sibutramine-induced c-Fos signals were largely confined to the cortex, amygdala and thalamus, which is consistent with the antidepressant, anxiolytic and analgesic action of dual serotonin-noradrenaline reuptake inhibitors [59–61]. Several weight-lowering compounds have glucoregulatory effects, which may involve central mechanisms of action independent of weight loss. Accordingly, rodent studies have suggested a role for the hypothalamus in the glucoregulatory effects of lorcaserin, rimonabant, bromocriptine and setmelanotide [9,62–65]. Furthermore, brain stem melanocortin neurocircuits have been implicated in the anti-diabetic action of 5-HT<sub>2C</sub> receptor and MC4R agonists [38,62,66]. Further studies are needed to determine whether glucoregulatory mechanisms contribute to the individual drug-induced c-Fos signatures.

It should be considered that drug-induced changes in whole-brain c-Fos architecture may represent composite signatures of both therapeutic and adverse effects. Components of the brainstem reticular formation, which integrates somatic and visceral inputs and subserves important autonomic, motor and cardiovascular functions [67], were activated by rimonabant, bromocriptine, sibutramine and setmelanotide. AP, NTS and CEA signalling have been implicated in visceral malaise, and enhanced NTS-CEA connectivity may be an important mechanism for GLP-1 receptor agonist-induced nausea responses [68]. Adverse central effects are not common with lorcaserin and bromocriptine treatment [69,70]. In contrast, rimonabant was withdrawn from the market in 2008 due to increased risk of neuropsychiatric adverse effects, notably depression and anxiety, which is consistent with prominent CB<sub>1</sub> receptor expression in brain areas associated with regulation of emotion such as the prefrontal cortex, hippocampus and amygdala [71]. In the current study, major components of the prefrontal cortex and amygdala were activated by rimonabant. Sibutramine was withdrawn from the market in 2010 because of cardiovascular safety concerns. Sibutramine was devoid of c-Fos effects in the

brainstem, supporting that haemodynamic responses to sibutramine are mediated by stimulation of peripheral adrenoceptor function [72]. Setmelanotide increases heart rate and blood pressure in rodents [73], but not in non-human primates and humans [74,75]. MC4R-induced cardiovascular effects in rodents have been linked to increased sympathetic activity in spinal pre-ganglionic neurons [66]. CNS accessibility may also be a critical factor for adverse cardiovascular effects of MC4R agonists [73].

Centrally acting weight-lowering drugs show very similar c-Fos signatures in lean and obese mice, making it useful to profile c-Fos expression signatures of weight-lowering compounds in lean mice. Accordingly, acute administration of semaglutide induces overall similar whole-brain c-Fos signature in lean and diet-induced obese (DIO) mice [18]. Although comparative c-Fos expression studies in lean and obese mice have not been reported for all compounds tested in the present study, conventional histological studies have demonstrated comparable c-Fos responses in lean and obese mice treated with 5-HT<sub>2C</sub> receptor agonists [76,77], CB<sub>1</sub> receptor antagonists [78,79] and MC4R agonists [80,81], respectively.

Drug doses were within ranges applied in mouse *in vivo* efficacy studies reported previously [38,40,82–86]. It should be emphasised that the drugs tested have different weight loss efficacy in both preclinical and clinical settings, which is determined by several factors, such as mode of action, pharmacokinetics, CNS drug and target distribution, as well as therapeutic index. The current study was not specifically designed to compare individual drug doses which would ultimately elicit similar weight loss. Temporal dynamics c-Fos expression should also be considered, as whole-brain c-Fos expression patterns were only determined two hours after dosing. For example, recent LSFM studies have demonstrated further anatomically restricted c-Fos signals four hours after semaglutide administration in lean mice [18,40]. A detailed profiling of time- and dose-response relationships on c-Fos expression could therefore further enable interpretation of the individual drug-induced brain activation signatures. Due to technical limitations, the current study cannot identify areas of inhibition. Other methods should be therefore employed to specifically delineate the various signalling pathways and neurocircuits recruited by centrally acting weight-lowering drugs.

## 5. CONCLUSION

In conclusion, we pinpoint several overlapping whole-brain activation signatures of various weight-lowering drugs. This shared feature suggests that weight-lowering drugs stimulate distinct homeostatic and non-homeostatic feeding centres. Future centrally acting anti-obesity compounds may be specifically designed to target key components of this neurocircuitry framework to provide more effective and sustained weight loss in obese patients.

## FUNDING

The work was funded by Innovation Fund Denmark (JP, grant number 8053-00121B).

## AUTHOR CONTRIBUTIONS

PB, NV, JJ and JHS conceived and designed the experiments. JHS, JP, UR, JLS, CGS, PB and DDT carried out the experiments. HHH, JP, UR, JLS, CGS, PB, KTGR, NV, JJ and JHS analysed and interpreted the data. HHH, JP, JLS, KTGR, JJ and JHS wrote the paper. All authors reviewed and approved the final paper.

## DATA AVAILABILITY

All data are accessible using the web-based imaging data viewer (G3DE, <https://g3de.gubra.dk>).

## ACKNOWLEDGEMENTS

N/A

## CONFLICT OF INTEREST

All authors are employed by Gubra; NV and JJ are owners of Gubra.

## REFERENCES

- [1] Clemmensen, C., Müller, T.D., Woods, S.C., Berthoud, H.-R., Seeley, R.J., Tschöp, M.H., 2017. Gut-brain cross-talk in metabolic control. *Cell* 168(5): 758–774. <https://doi.org/10.1016/j.cell.2017.01.025>.
- [2] Berthoud, H.R., Münzberg, H., Morrison, C.D., 2017. Blaming the brain for obesity: integration of hedonic and homeostatic mechanisms. *Gastroenterology* 152(7):1728–1738. <https://doi.org/10.1053/j.gastro.2016.12.050>.
- [3] Hoyda, T.D., Smith, P.M., Ferguson, A.V., 2009. Gastrointestinal hormone actions in the central regulation of energy metabolism: potential sensory roles for the circumventricular organs. *International Journal of Obesity* 33:S16–S21. <https://doi.org/10.1038/ijo.2009.11>.
- [4] Caron, A., Richard, D., 2017. Neuronal systems and circuits involved in the control of food intake and adaptive thermogenesis. *Annals of the New York Academy of Sciences*, 35–53. <https://doi.org/10.1111/nyas.13263>.
- [5] Tulloch, A.J., Murray, S., Vaicekonyte, R., Avena, N.M., 2015. Neural responses to macronutrients: hedonic and homeostatic mechanisms. *Gastroenterology* 148(6):1205–1218. <https://doi.org/10.1053/j.gastro.2014.12.058>.
- [6] Berthoud, H.-R., Lenard, N.R., Shin, A.C., 2011. Food reward, hyperphagia, and obesity. *American Journal of Physiology - Regulatory, Integrative and Comparative Physiology* 300(6):R1266–R1277.
- [7] Ferrario, C.R., Labouébe, G., Liu, S., Nieh, E.H., Routh, V.H., Xu, S., et al., 2016. Homeostasis meets motivation in the battle to control food intake. *Journal of Neuroscience* 36:11469–11481. *Society for Neuroscience*.
- [8] Farr, O.M., Li, C.S.R., Mantzoros, C.S., 2016. Central nervous system regulation of eating: insights from human brain imaging. *Metabolism: Clinical and Experimental*, 699–713. <https://doi.org/10.1016/j.metabol.2016.02.002>.
- [9] Gautron, L., Elmquist, J.K., Williams, K.W., 2015. Neural control of energy balance: translating circuits to therapies. *Cell*, 133–145. <https://doi.org/10.1016/j.cell.2015.02.023>.
- [10] Coulter, A.A., Rebello, C.J., Greenway, F.L., 2018. Centrally acting agents for obesity: past, present, and future. *Drugs*, 1113–1132. <https://doi.org/10.1007/s40265-018-0946-y>.
- [11] Dietrich, M.O., Horvath, T.L., 2012. Limitations in anti-obesity drug development: the critical role of hunger-promoting neurons. *Nature Reviews Drug Discovery* 11(9):675–691. <https://doi.org/10.1038/nrd3739>.
- [12] Khera, R., Murad, M.H., Chandar, A.K., Dulai, P.S., Wang, Z., Prokop, L.J., et al., 2016. Association of pharmacological treatments for obesity with weight loss and adverse events: a systematic review and meta-analysis. *JAMA - Journal of the American Medical Association* 315(22):2424–2434. <https://doi.org/10.1001/jama.2016.7602>.
- [13] Srivastava, G., Apovian, C., 2018. Future pharmacotherapy for obesity: new anti-obesity drugs on the horizon. *Current Obesity Reports*, 147–161. <https://doi.org/10.1007/s13679-018-0300-4>.
- [14] Farivar, R., Zangenehpour, S., Chaudhuri, A., 2004. Cellular-resolution activity mapping of the brain using immediate-early gene expression. *Frontiers in Bioscience*, 104–109. <https://doi.org/10.2741/1198>.
- [15] Cincotta, A.H., Meier, A.H., 1996. Bromocriptine (Ergoset) reduces body weight and improves glucose tolerance in obese subjects. *Diabetes Care* 19(6):667–670. <https://doi.org/10.2337/diacare.19.6.667>.
- [16] Renier, N., Wu, Z., Simon, D.J., Yang, J., Ariel, P., Tessier-Lavigne, M., 2014. iDISCO: a simple, rapid method to immunolabel large tissue samples for volume imaging. *Cell* 159(4):896–910. <https://doi.org/10.1016/j.cell.2014.10.010>.
- [17] Renier, N., Adams, E.L., Kirst, C., Dulac, C., Osten, P., Tessier-Lavigne, M., 2016. Mapping of brain activity by automated volume Analysis of immediate early genes. *Cell* 165(7):1789–1802. <https://doi.org/10.1016/j.cell.2016.05.007>.
- [18] Perens, J., Salinas, C.G., Skytte, J.L., Roostalu, U., Dahl, A.B., Dyrby, T.B., et al., 2020. An optimized mouse brain atlas for automated mapping and quantification of neuronal activity using iDISCO+ and light sheet fluorescence microscopy. *Neuroinformatics*. <https://doi.org/10.1007/s12021-020-09490-8>.
- [19] Klein, S., Staring, M., Murphy, K., Viergever, M.A., Pluim, J.P.W., 2010. elastic: a toolbox for intensity-based medical image registration. *IEEE Transactions on Medical Imaging* 29(1):196–205. <https://doi.org/10.1109/TMI.2009.2035616>.
- [20] Shamonin, D.P., Bron, E.E., Lelieveldt, B.P.F., Smits, M., Klein, S., Staring, M., 2014. Fast parallel image registration on CPU and GPU for diagnostic classification of Alzheimer's disease. *Frontiers in Neuroinformatics* 7:50. <https://doi.org/10.3389/fninf.2013.00050>.
- [21] Wang, Q., Ding, S.L., Li, Y., Royall, J., Feng, D., Lesnar, P., et al., 2020. The allen mouse brain common coordinate framework: a 3D reference atlas. *Cell* 181(4):936–953. <https://doi.org/10.1016/j.cell.2020.04.007> e20.
- [22] R Core Team, 2018. *R: a language and environment for statistical computing*. Vienna, Austria.
- [23] Venables, W., Ripley, B., 2002. *Modern applied statistics with S*. New York, USA: Springer. Fourth.
- [24] Hothorn, T., Bretz, F., Westfall, P., 2008. Simultaneous inference in general parametric models. *Biometrical Journal* 50(3):346–363.
- [25] Zeileis, A., Hothorn, T., 2002. Diagnostic checking in regression relationships. *R News* 2(3):7–10.
- [26] Fox, J., Weisberg, S., 2019. *An R companion to applied regression*. Thousand Oaks, CA, USA: Sage. Third.
- [27] Vandenberghe, M.E., Souedet, N., Hérard, A.S., Ayrat, A.M., Letronne, F., Balbastre, Y., et al., 2018. Voxel-based statistical analysis of 3D immunostained tissue imaging. *Frontiers in Neuroscience* 12(754). <https://doi.org/10.3389/fnins.2018.00754>.
- [28] Spisák, T., Spisák, Z., Zunhammer, M., Bingel, U., Smith, S., Nichols, T., et al., 2018. Probabilistic TFCE: a generalized combination of cluster size and voxel intensity to increase statistical power. *NeuroImage* 185:12–26. <https://doi.org/10.1016/j.neuroimage.2018.09.078>.
- [29] Berthoud, H.R., 2008. The vagus nerve, food intake and obesity. *Regulatory Peptides*, 15–25. <https://doi.org/10.1016/j.regpep.2007.08.024>.
- [30] Roman, C.W., Derkach, V.A., Palmiter, R.D., 2016. Genetically and functionally defined NTS to PBN brain circuits mediating anorexia. *Nature Communications* 7. <https://doi.org/10.1038/ncomms11905>.
- [31] Carter, M.E., Soden, M.E., Zweifel, L.S., Palmiter, R.D., 2013. Genetic identification of a neural circuit that suppresses appetite. *Nature* 503(7474):111–114. <https://doi.org/10.1038/nature12596>.
- [32] Zséli, G., Vida, B., Martinez, A., Lechan, R.M., Khan, A.M., Fekete, C., 2016. Elucidation of the anatomy of a satiety network: focus on connectivity of the parabrachial nucleus in the adult rat. *Journal of Comparative Neurology* 524(14):2803–2827. <https://doi.org/10.1002/cne.23992>.
- [33] Simpson, K.A., Martin, N.M., Bloom, S.R., 2008. Hypothalamic regulation of appetite. *Expert Review of Endocrinology and Metabolism*, 577–592. <https://doi.org/10.1586/17446651.3.5.577>.
- [34] Barbier, M., Chometton, S., Pautrat, A., Miguet-Alfonsi, C., Datiche, F., Gascuel, J., et al., 2020. A basal ganglia-like corticula-amygdalora-hypothalamic network mediates feeding behavior. *Proceedings of the National*

- Academy of Sciences of the United States of America 117(27):15967–15976. <https://doi.org/10.1073/pnas.2004914117>.
- [35] Le May, M.V., Hume, C., Sabatier, N., Schéle, E., Bake, T., Bergström, U., et al., 2019. Activation of the rat hypothalamic supramammillary nucleus by food anticipation, food restriction or ghrelin administration. *Journal of Neuroendocrinology* 31(7). <https://doi.org/10.1111/jne.12676>.
- [36] Blouet, C., Schwartz, G.J., 2010. Hypothalamic nutrient sensing in the control of energy homeostasis. *Behavioural Brain Research*, 1–12. <https://doi.org/10.1016/j.bbr.2009.12.024>.
- [37] Garfield, A.S., Lam, D.D., Marston, O.J., Przydzial, M.J., Heisler, L.K., 2009. Role of central melanocortin pathways in energy homeostasis. *Trends in Endocrinology and Metabolism*, 203–215. <https://doi.org/10.1016/j.tem.2009.02.002>.
- [38] D'Agostino, G., Lyons, D., Cristiano, C., Lettieri, M., Olarte-Sanchez, C., Burke, L.K., et al., 2018. Nucleus of the solitary tract serotonin 5-HT2C receptors modulate food intake. *Cell Metabolism* 28(4):619–630. <https://doi.org/10.1016/j.cmet.2018.07.017> e5.
- [39] Baldini, G., Phelan, K.D., 2019. The melanocortin pathway and control of appetite-progress and therapeutic implications. *Journal of Endocrinology*, R1–R33. <https://doi.org/10.1530/JOE-18-0596>.
- [40] Gabery, S., Salinas, C.G., Paulsen, S.J., Ahnfelt-Rønne, J., Alanentalo, T., Baquero, A.F., et al., 2020. Semaglutide lowers body weight in rodents via distributed neural pathways. *JCI Insight* 5(6). <https://doi.org/10.1172/jci.insight.133429>.
- [41] Vertes, R.P., Linley, S.B., Hoover, W.B., 2015. Limbic circuitry of the midline thalamus. *Neuroscience & Biobehavioral Reviews*, 89–107. <https://doi.org/10.1016/j.neubiorev.2015.01.014>.
- [42] Samuelsen, C.L., Gardner, M.P.H., Fontanini, A., 2013. Thalamic contribution to cortical processing of taste and expectation. *Journal of Neuroscience* 33(5): 1815–1827. <https://doi.org/10.1523/JNEUROSCI.4026-12.2013>.
- [43] Stuber, G.D., Wise, R.A., 2016. Lateral hypothalamic circuits for feeding and reward. *Nature Neuroscience*, 198–205. <https://doi.org/10.1038/nn.4220>.
- [44] Terem, A., Gonzales, B.J., Peretz-Rivlin, N., Ashwal-Fluss, R., Bleistein, N., del Mar Reus-Garcia, M., et al., 2020. Claustral neurons projecting to frontal cortex mediate contextual association of reward. *Current Biology*. <https://doi.org/10.1016/j.cub.2020.06.064>.
- [45] Kanoski, S.E., Hayes, M.R., Skibicka, K.P., 2016. GLP-1 and weight loss: unraveling the diverse neural circuitry 310(10):R885–R895. <https://doi.org/10.1152/ajpregu.00520.2015>.
- [46] Koch, M., 2017. Cannabinoid receptor signaling in central regulation of feeding behavior: a mini-review. *Frontiers in Neuroscience*. <https://doi.org/10.3389/fnins.2017.00293>.
- [47] Ellacott, K.L.J., Cone, R.D., 2004. The central melanocortin system and the integration of short- and long-term regulators of energy homeostasis. *Recent Progress in Hormone Research*, 395–408. <https://doi.org/10.1210/rp.59.1.395>.
- [48] Secher, A., Jelsing, J., Baquero, A.F., Hecksher-Sørensen, J., Cowley, M.A., Dalbøge, L.S., et al., 2014. The arcuate nucleus mediates GLP-1 receptor agonist liraglutide-dependent weight loss. *Journal of Clinical Investigation* 124(10):4473–4488. <https://doi.org/10.1172/JCI75276>.
- [49] Sisley, S., Gutierrez-Aguilar, R., Scott, M., D'Alessio, D.A., Sandoval, D.A., Seeley, R.J., 2014. Neuronal GLP1R mediates liraglutide's anorectic but not glucose-lowering effect. *Journal of Clinical Investigation* 124(6): 2456–2463.
- [50] Adams, J.M., Pei, H., Sandoval, D.A., Seeley, R.J., Chang, R.B., Liberles, S.D., et al., 2018. Liraglutide modulates appetite and body weight through glucagon-like peptide 1 receptor-expressing glutamatergic neurons. *Diabetes* 67:1538–1548. American Diabetes Association Inc.
- [51] Müller, T.D., Finan, B., Bloom, S.R., D'Alessio, D., Drucker, D.J., Flatt, P.R., et al., 2019. Glucagon-like peptide 1 (GLP-1). *Molecular Metabolism*, 72–130. <https://doi.org/10.1016/j.molmet.2019.09.010>.
- [52] Ong, Z.Y., Liu, J.J., Pang, Z.P., Grill, H.J., 2017. Paraventricular thalamic control of food intake and reward: role of glucagon-like peptide-1 receptor signaling. *Neuropsychopharmacology* 42(12):2387–2397. <https://doi.org/10.1038/npp.2017.150>.
- [53] Davis, L.M., Michaelides, M., Cheskin, L.J., Moran, T.H., Aja, S., Watkins, P.A., et al., 2009. Bromocriptine administration reduces hyperphagia and adiposity and differentially affects dopamine D2 receptor and transporter binding in leptin-receptor-deficient Zucker rats and rats with diet-induced obesity. *Neuroendocrinology* 89(2):152–162.
- [54] Folgueira, C., Beiroa, D., Porteiro, B., Duquenne, M., Puighermanal, E., Fondevila, M.F., et al., 2019. Hypothalamic dopamine signalling regulates brown fat thermogenesis. *Nature Metabolism* 1(8):811–829. <https://doi.org/10.1038/s42255-019-0099-7>.
- [55] Higgins, G.A., Zeeb, F.D., Fletcher, P.J., 2017. Role of impulsivity and reward in the anti-obesity actions of 5-HT2C receptor agonists. *Journal of Psychopharmacology*, 1403–1418. <https://doi.org/10.1177/0269881117735797>.
- [56] Melis, T., Succu, S., Sanna, F., Boi, A., Argiolas, A., Melis, M.R., 2007. The cannabinoid antagonist SR 141716A (Rimonabant) reduces the increase of extra-cellular dopamine release in the rat nucleus accumbens induced by a novel high palatable food. *Neuroscience Letters* 419(3):231–235. <https://doi.org/10.1016/j.neulet.2007.04.012>.
- [57] Pandit, R., Omrani, A., Luijendijk, M.C.M., De Vrind, V.A.J., Van Rozen, A.J., Ophuis, R.J.A.O., et al., 2016. Melanocortin 3 receptor signaling in midbrain dopamine neurons increases the motivation for food reward. *Neuropsychopharmacology* 41(9):2241–2251. <https://doi.org/10.1038/npp.2016.19>.
- [58] Jackson, H.C., Bearham, M.C., Hutchins, L.J., Mazurkiewicz, S.E., Needham, A.M., Heal, D.J., 1997. Investigation of the mechanisms underlying the hypophagic effects of the 5-HT and noradrenaline reuptake inhibitor, sibutramine, in the rat. *British Journal of Pharmacology* 121(8):1613–1618. <https://doi.org/10.1038/sj.bjp.0701311>.
- [59] Bravo, L., Llorca-Torralla, M., Berrocoso, E., Micó, J.A., 2019. Monoamines as drug targets in chronic pain: focusing on neuropathic pain. *Frontiers in Neuroscience*. <https://doi.org/10.3389/fnins.2019.01268>.
- [60] Papakostas, G.I., Thase, M.E., Fava, M., Nelson, J.C., Shelton, R.C., 2007. Are antidepressant drugs that combine serotonergic and noradrenergic mechanisms of action more effective than the selective serotonin reuptake inhibitors in treating major depressive disorder? A meta-analysis of studies of newer agents. *Biological Psychiatry* 62(11):1217–1227. <https://doi.org/10.1016/j.biopsych.2007.03.027>.
- [61] Kornstein, S.G., Russell, J.M., Spann, M.E., Crits-Christoph, P., Ball, S.G., 2009. Duloxetine in the treatment of generalized anxiety disorder. *Expert Review of Neurotherapeutics*, 155–165. <https://doi.org/10.1586/14737175.9.2.155>.
- [62] Burke, L.K., Ogunnowo-Bada, E., Georgescu, T., Cristiano, C., de Morentin, P.B.M., Valencia Torres, L., et al., 2017. Lorcaserin improves glycemic control via a melanocortin neurocircuit. *Molecular Metabolism* 6(10): 1092–1102. <https://doi.org/10.1016/j.molmet.2017.07.004>.
- [63] Kumar, K.G., Sutton, G.M., Dong, J.Z., Roubert, P., Plas, P., Halem, H.A., et al., 2009. Analysis of the therapeutic functions of novel melanocortin receptor agonists in MC3R- and MC4R-deficient C57BL/6J mice. *Peptides* 30(10): 1892–1900. <https://doi.org/10.1016/j.peptides.2009.07.012>.
- [64] O'Hare, J.D., Zielirski, E., Cheng, B., Scherer, T., Buettner, C., 2011. Central endocannabinoid signaling regulates hepatic glucose production and systemic lipolysis. *Diabetes* 60(4):1055–1062. <https://doi.org/10.2337/db10-0962>.
- [65] Furigo, I.C., Suzuki, M.F., Oliveira, J.E., Ramos-Lobo, A.M., Teixeira, P.D.S., Pedrosa, J.A., et al., 2019. Suppression of prolactin secretion partially explains the antidiabetic effect of bromocriptine in ob/ob Mice. *Endocrinology* 160(1): 193–204. <https://doi.org/10.1210/en.2018-00629>.
- [66] Sohn, J.W., Harris, L.E., Berglund, E.D., Liu, T., Vong, L., Lowell, B.B., et al., 2013. Melanocortin 4 receptors reciprocally regulate sympathetic and parasympathetic preganglionic neurons. *Cell* 152(3):612–619. <https://doi.org/10.1016/j.cell.2012.12.022>.

- [67] Yates, B.J., Stocker, S.D., 1998. Integration of somatic and visceral inputs by the brainstem. Functional considerations. *Experimental Brain Research*, 269–275. <https://doi.org/10.1007/s002210050342>.
- [68] Kanoski, S.E., Rupperecht, L.E., Fortin, S.M., De Jonghe, B.C., Hayes, M.R., 2012. The role of nausea in food intake and body weight suppression by peripheral GLP-1 receptor agonists, exendin-4 and liraglutide. *Neuropharmacology* 62(5–6):1916–1927.
- [69] Tchang, B.G., Abel, B., Zecca, C., Saunders, K.H., Shukla, A.P., 2020. An up-to-date evaluation of lorcaserin hydrochloride for the treatment of obesity. *Expert Opinion on Pharmacotherapy* 21(1):21–28. <https://doi.org/10.1080/14656566.2019.1685496>.
- [70] Lamos, E.M., Levitt, D.L., Munir, K.M., 2016. A review of dopamine agonist therapy in type 2 diabetes and effects on cardio-metabolic parameters. *Primary Care Diabetes*, 60–65. <https://doi.org/10.1016/j.pcd.2015.10.008>.
- [71] Mackie, K., 2005. *Distribution of cannabinoid receptors in the central and peripheral nervous system*. *Cannabinoids*. Springer-Verlag. p. 299–325.
- [72] Birkenfeld, A.L., Schroeder, C., Boschmann, M., Tank, J., Franke, G., Luft, F.C., et al., 2002. Paradoxical effect of sibutramine on autonomic cardiovascular regulation. *Circulation* 106(19):2459–2465. <https://doi.org/10.1161/01.CIR.0000036370.31856.73>.
- [73] Sharma, S., Garfield, A.S., Shah, B., Kleyn, P., Ichetovkin, I., Moeller, I.H., et al., 2019. Current mechanistic and pharmacodynamic understanding of melanocortin-4 receptor activation. *Molecules*. <https://doi.org/10.3390/molecules24101892>.
- [74] Collet, T.H., Dubern, B., Mokrosinski, J., Connors, H., Keogh, J.M., Mendes de Oliveira, E., et al., 2017. Evaluation of a melanocortin-4 receptor (MC4R) agonist (Setmelanotide) in MC4R deficiency. *Molecular Metabolism* 6(10): 1321–1329. <https://doi.org/10.1016/j.molmet.2017.06.015>.
- [75] Kievit, P., Halem, H., Marks, D.L., Dong, J.Z., Glavas, M.M., Sinnayah, P., et al., 2013. Chronic treatment with a melanocortin-4 receptor agonist causes weight loss, reduces insulin resistance, and improves cardiovascular function in diet-induced obese rhesus macaques. *Diabetes* 62(2):490–497. <https://doi.org/10.2337/db12-0598>.
- [76] Doslíkova, B., Garfield, A.S., Shaw, J., Evans, M.L., Burdakov, D., Billups, B., et al., 2013. 5-HT<sub>2C</sub> receptor agonist anorectic efficacy potentiated by 5-HT<sub>1B</sub> receptor agonist coapplication: an effect mediated via increased proportion of pro-opiomelanocortin neurons activated. *Journal of Neuroscience* 33(23): 9800–9804. <https://doi.org/10.1523/JNEUROSCI.4326-12.2013>.
- [77] Zhou, L., Sutton, G.M., Rochford, J.J., Semple, R.K., Lam, D.D., Oksanen, L.J.J., et al., 2007. Serotonin 2C receptor agonists improve type 2 diabetes via melanocortin-4 receptor signaling pathways. *Cell Metabolism* 6(5):398–405. <https://doi.org/10.1016/j.cmet.2007.10.008>.
- [78] Tam, J., Szanda, G., Drori, A., Liu, Z., Cinar, R., Kashiwaya, Y., et al., 2017. Peripheral cannabinoid-1 receptor blockade restores hypothalamic leptin signaling. *Molecular Metabolism* 6(10):1113–1125. <https://doi.org/10.1016/j.molmet.2017.06.010>.
- [79] Sinnayah, P., Jobst, E.E., Rathner, J.A., Caldera-Siu, A.D., Tonelli-Lemos, L., Eusterbrock, A.J., et al., 2008. Feeding induced by cannabinoids is mediated independently of the melanocortin system. *PLoS One* 3(5). <https://doi.org/10.1371/journal.pone.0002202>.
- [80] Rowland, N.E., Schaub, J.W., Robertson, K.L., Andreasen, A., Haskell-Luevano, C., 2010. Effect of MTII on food intake and brain c-Fos in melanocortin-3, melanocortin-4, and double MC3 and MC4 receptor knockout mice. *Peptides* 31(12):2314–2317. <https://doi.org/10.1016/j.peptides.2010.08.016>.
- [81] Benoit, S.C., Schwartz, M.W., Lachey, J.L., Hagan, M.M., Rushing, P.A., Blake, K.A., et al., 2000. A novel selective melanocortin-4 receptor agonist reduces food intake in rats and mice without producing aversive consequences. *Journal of Neuroscience* 20(9):3442–3448. <https://doi.org/10.1523/jneurosci.20-09-03442.2000>.
- [82] Lau, J., Bloch, P., Schäffer, L., Pettersson, I., Spetzler, J., Kofoed, J., et al., 2015. Discovery of the once-weekly glucagon-like peptide-1 (GLP-1) analogue semaglutide. *Journal of Medicinal Chemistry* 58(18):7370–7380. <https://doi.org/10.1021/acs.jmedchem.5b00726>.
- [83] Clemmensen, C., Finan, B., Fischer, K., Tom, R.Z., Legutko, B., Seherer, L., et al., 2015. Dual melanocortin-4 receptor and GLP-1 receptor agonism amplifies metabolic benefits in diet-induced obese mice. *EMBO Molecular Medicine* 7(3):288–298. <https://doi.org/10.15252/emmm.201404508>.
- [84] Trillou, C.R., Arnone, M., Delgorge, C., Gonalons, N., Keane, P., Maffrand, J.P., et al., 2003. Anti-obesity effect of SR141716, a CB1 receptor antagonist, in diet-induced obese mice. *American Journal of Physiology - Regulatory, Integrative and Comparative Physiology* 284(2 53–2). <https://doi.org/10.1152/ajpregu.00545.2002>.
- [85] Cincotta, A.H., Tozzo, E., Scislowski, P.W.D., 1997. Bromocriptine/SKF38393 treatment ameliorates obesity and associated metabolic dysfunctions in obese (ob/ob) mice. *Life Sciences* 61(10):951–956. [https://doi.org/10.1016/S0024-3205\(97\)00599-7](https://doi.org/10.1016/S0024-3205(97)00599-7).
- [86] Mashiko, S., Ishihara, A., Iwaasa, H., Moriya, R., Kitazawa, H., Mitobe, Y., et al., 2008. Effects of a novel Y5 antagonist in obese mice: combination with food restriction or sibutramine. *Obesity* 16(7):1510–1515. <https://doi.org/10.1038/oby.2008.223>.